Inorg. Chem. **2008**, *47*, 7588−7598

Metallo-Supramolecular Self-Assembly: the Case of Triangle-Square Equilibria

Torsten Weilandt,[†,‡] Ralf W. Troff,[†] Heidi Saxell,[§,||] Kari Rissanen,[§] and Christoph A. Schalley*[,†]

Institut für Chemie and Biochemie - Organische Chemie, Freie Universität Berlin, Germany, Kekulé-Institut für Organische Chemie and Biochemie der Universität Bonn, Germany, and Department of Chemistry, Nanoscience Center, University of Jyväskylä, Finland

Received February 21, 2008

For the efficient self-assembly of metallo-supramolecular complexes, not only reversibility is required but also two other properties have to be controlled as well: (i) The right binding sites need to be programmed into the building blocks at the appropriate positions. (ii) The building blocks must be rigid enough to support the geometrical arrangement and to avoid the unfavorable entropy effects connected with the conformational fixation of flexible molecules. A series of different bis-pyridyl ligands is reported which self-assemble with (dppp)M(OTf)$_2$ complexes (dppp = 1,3-bis-(diphenylphosphino)propane; M = Pd^{II}, Pt^{II}) to yield squares and/or triangles as the products. Enthalpic contributions (higher strain in the triangle) and entropic contributions (higher number of triangles from the same building blocks) determine the equilibrium. The effects of concentration, temperature, and solvent properties on the equilibrium have been studied. To characterize the complexes under study, a combination of ^{1}H, ^{31}P, and diffusion-ordered NMR spectroscopy, electrospray-ionization Fourier-transform ion-cyclotron-resonance mass spectrometry, and X-ray crystallography is needed. Variable-temperature NMR spectroscopy provides evidence for fast ligand-exchange processes occurring for the Pd complexes, while the Pt complexes exchange ligands much more slowly.

Introduction

Since the early 1990s, when Fujita[1] and Stang[2] presented the first metallo-supramolecular squares, a large number of self-assembled metal-containing supramolecular structures have been reported.[3] Different geometries of self-assembled structures are available by variation of the metal complexes and the ligands, among them polyhedra, which are able to encapsulate guests and to mediate reactions inside their cavities.[4] If *cis*-blocked square-planar metal centers are used in combination with linear bidentate ligands with two diametrically diverging binding sites, squares[3,5] or triangles[6] with the metal centers on the corners and the ligands on the edges are the favored structures. With *trans*-blocked or linearly coordinating metal centers and bent ligands, squares or triangles with metal centers on the edges and ligands as corner elements were obtained.[7] Beside these, also other types of triangles and squares are known.[8]

If linear rigid bis-pyridyl ligands are self-assembled with square-planar (dppp)M(OTf)$_2$ corners (dppp = 1,3-bis-diphenylphosphinopropane; M = Pd^{II}, Pt^{II}), the ratio of squares and triangles[9,10] is determined by a sensitive balance between entropy and enthalpy. While entropy favors the formation of triangles, since a larger number of particles is formed from the same number of building blocks, enthalpy favors the formation of squares because ring strain is then minimized. Because of this balance, triangles become the major component in an equilibrium if the ligand′s flexibility reduces the strain by allowing the ligand to bend. Squares become the major component of the mixture if the ligands are sufficiently rigid so that the enthalpic benefit overcompensates the entropic penalty in square formation. There exist, however, a few reports[11] on such equilibria, where entropy drives the formation of the larger assembly, probably because of solvation effects. The equilibria between triangles and squares also depend on the metal center and its ancillary

* To whom correspondence should be addressed. E-mail: schalley@chemie.fu-berlin.de. Phone: ++49-30-83852639. Fax: ++49-30-83856612.
† Freie Universität Berlin.
‡ Kekulé-Institut für Organische Chemie and Biochemie der Universität Bonn.
§ University of Jyväskylä.
|| Present address: BASF-AG, Ludwigshafen, Germany.

10.1021/ic800334k CCC: $40.75
Published on Web 08/05/2008

ligand, which can influence the equilibria by its electronic and steric effects.[10] For example, the steric repulsion of the bipyridine attached to (2,2′-bipyridine)Pd^{II} corners has been described to provoke the formation of triangles and squares, where the corresponding ethylene diamine complexes exclusively form squares.[12] As initially suggested by Fujita[12] and later proved by Long[13] et al., an equilibrium between squares and triangles based on rigid 4,4′-bipyridine ligands can be observed when ruthenium metal-centers and 4,4′-bipyridine were used as building blocks. In this case, the octahedral coordination sphere of the ruthenium corners is so flexible that it allows an $N_{bipy}-Ru-N_{bipy}$ angle of 83.7°, reducing the strain of the triangle. In addition to this, some of the strain of the triangle is compensated for by bending the 4,4′-bipyridines.

A mixture of (dppp)$M(OTf)_2$ ($M = Pd^{II}$, Pt^{II}) as corner element and 4,4′-bipyridine as the edge ligand self-assembles to yield squares as the only compound present in solution[2] because 4,4′-bipyridine is not flexible enough to sufficiently reduce the ring tension in triangles. With longer and more flexible ligands like dipyridyl ethylene or azopyridine, an equilibrium between triangles and squares exists.[9d] However, in the absence of ligand exchange equilibria, that is, under the environment-free conditions in the high vacuum of a mass spectrometer, bipyridine squares with (dppp)Pt^{II} corners have been observed to fragment into triangles through a supramolecular analogue of a neighboring group effect.[9d,14] Consequently, under these particular conditions, even bipyridine may yield triangles.

The characterization of these equilibria often raises analytical problems. For X-ray crystal structure analysis, suitable single crystals are often difficult to obtain. However, even the analysis of high-quality single crystals may mislead if one of the compounds in solution crystallizes preferentially followed by readjustment of the solution equilibrium. Thus, the crystal structure data cannot always be extrapolated to the solution situation. In the NMR spectra, small shift differences, signal superposition, or fast exchange equilibria[15] may become problematic. Sometimes, aggregation results in

(1) Fujita, M.; Yazaki, J.; Ogura, K. *J. Am. Chem. Soc.* **1990**, *112*, 5645–5647.

(2) (a) Stang, P. J.; Cao, D. H. *J. Am. Chem. Soc.* **1994**, *116*, 4981–4982. Also see: (b) Stang, P. J.; Zhdankin, V. V. *J. Am. Chem. Soc.* **1993**, *115*, 9808–9809.

(3) For reviews on polynuclear, self-assembling metal complexes, see: (a) Leininger, S.; Olenyuk, B.; Stang, P. J. *Chem. Rev.* **2000**, *100*, 853–908. (b) Holliday, B. J.; Mirkin, C. A. *Angew. Chem.* **2001**, *113*, 2076–2097. *Angew. Chem., Int. Ed.* **2001**, *40*, 2022−2043. (c) Albrecht, M. *Chem. Rev.* **2001**, *101*, 3457–3498. (d) Cotton, F. A.; Lin, C.; Murillo, C. A. *Acc. Chem. Res.* **2001**, *34*, 759–771. (e) Sun, S.-S.; Lees, A. J. *Coord. Chem. Rev.* **2002**, *230*, 170–192. (f) Würthner, F.; You, C.-C.; Saha-Möller, C. R. *Chem. Soc. Rev.* **2004**, *33*, 133–146. (g) Hofmeier, H.; Schubert, U. S. *Chem. Soc. Rev.* **2004**, *33*, 373–399. (h) Fujita, M.; Tominaga, M.; Hori, A.; Therrien, B. *Acc. Chem. Res.* **2005**, *38*, 369–380. (i) Kaiser, A.; Bäuerle, P. *Top. Curr. Chem.* **2005**, *249*, 127–201. (j) You, C.-C.; Dobrawa, R.; Saha-Möller, C. R.; Würthner, F. *Top. Curr. Chem.* **2005**, *258*, 39–82. (k) Nitschke, J. R. *Acc. Chem. Res.* **2007**, *40*, 103–112. (l) Georgiev, I. G.; MacGillivray, L. R. *Chem. Soc. Rev.* **2007**, *36*, 1239–1248. (m) Gunnlaugsson, T.; Stomeo, F. *Org. Biomol. Chem.* **2007**, *5*, 1999–2009.

(4) For selected recent examples, see: (a) Müller, I. M.; Möller, D.; Schalley, C. A. *Angew. Chem.* **2005**, *117*, 485–488. *Angew. Chem., Int. Ed.* **2005**, *44*, 480−484. (b) Yoshizawa, M.; Sato, N.; Fujita, M. *Chem. Lett.* **2005**, *34*, 1392–1393. (c) Amouri, H.; Mimassi, L.; Rager, M. N.; Mann, B. E.; Guyard-Duhayon, C.; Raehm, L. *Angew. Chem.* **2005**, *117*, 4619–4622. *Angew. Chem., Int. Ed.* **2005**, *44*, 4543−4546. (d) Tashiro, S.; Tominaga, M.; Yamaguchi, Y.; Kato, K.; Fujita, M. *Angew. Chem.* **2006**, *118*, 247–250; *Angew. Chem., Int. Ed.* **2006**, *45*, 241−244. (e) Fiedler, D.; Bergman, R. G.; Raymond, K. N. *Angew. Chem.* **2006**, *118*, 759–762; *Angew. Chem., Int. Ed.* **2006**, *45*, 745−748. (f) Das, S.; Bharadwaj, P. K. *Inorg. Chem.* **2006**, *45*, 5257–5259. (g) Albrecht, M.; Janser, I.; Burk, S.; Weis, P. *Dalton Trans.* **2006**, 2875–2880. (h) Haino, T.; Kobayashi, M.; Fukazawa, Y. *Chem.−Eur. J.* **2006**, *12*, 3310–3319. (i) Pluth, M. D.; Berman, R. G.; Raymond, K. N. *Chem. Soc. Rev.* **2007**, *36*, 161–171. (j) Tashiro, K.; Aida, T. *Chem. Soc. Rev.* **2007**, *36*, 189–197. (k) Pluth, M. D.; Berman, R. G.; Raymond, K. N. *Science* **2007**, *316*, 85–88. (l) John, R. P.; Moon, D.; Lah, M. S. *Supramol. Chem.* **2007**, *19*, 295–308. (m) Leung, D. H.; Berman, R. G.; Raymond, K. N. *J. Am. Chem. Soc.* **2007**, *129*, 2746–2747. (n) Pluth, M. D.; Berman, R. G.; Raymond, K. N. *J. Am. Chem. Soc.* **2007**, *129*, 11459–11467.

(5) For examples of metallo-supramolecular squares, see: (a) Stang, P. J.; Whiteford, J. A. *Organometallics* **1994**, *13*, 3776–3777. (b) Slone, R. V.; Yoon, D. I.; Calburn, R. M.; Hupp, J. T. *J. Am. Chem. Soc.* **1995**, *117*, 11813–11814. (c) Würthner, F.; Sautter, A.; Schmid, D.; Weber, P. J. A. *Chem.−Eur. J.* **2001**, *7*, 894–902. (d) Sun, S.-S.; Lees, A. J. *Inorg. Chem.* **2001**, *40*, 3154–3160. (e) Safarowsky, C.; Merz, L.; Rang, A.; Broekmann, P.; Herrmann, B. A.; Schalley, C. A. *Angew. Chem.* **2004**, *116*, 1311–1314; *Angew. Chem., Int. Ed.* **2004**, *43*, 1291−1294. (f) Janka, M.; Anderson, G. K.; Rath, N. P. *Organometallics* **2004**, *23*, 4382–4390. (g) Lee, S. J.; Kim, J. S.; Lin, W. *Inorg. Chem.* **2004**, *43*, 6579–6588. (h) Cheng, K. F.; Thai, N. A.; Teague, L. C.; Grohmanna, K.; Drain, C. M. *Chem. Commun.* **2005**, *37*, 4678–4680. (i) Jiang, L.; Lu, T. B.; Feng, X.-L. *Inorg. Chem.* **2005**, *44*, 7056–7062. (j) Kraft, S.; Hanuschek, E.; Beckhaus, R.; Haase, D.; Saak, W. *Chem.−Eur. J.* **2005**, *11*, 969–978. (k) Abrahams, F. B.; Price, D. J.; Robson, R. *Angew. Chem.* **2006**, *118*, 820–824; *Angew. Chem., Int. Ed.* **2006**, *45*, 806−810. (l) Cotton, F. A.; Liu, C. Y.; Murillo, C. A.; Wang, X. *Inorg. Chem.* **2006**, *45*, 2619–2626. (m) You, C.-C.; Hippius, C.; Grüne, M.; Würthner, F. *Chem.−Eur. J.* **2006**, *12*, 7510–7519. (n) Fyles, T. M.; Tong, C. C. *New J. Chem.* **2007**, *31*, 296–304. (o) Mounir, M.; Lorenzo, J.; Ferrer, M.; Prieto, M. J.; Rossell, O.; Avilès, F. X.; Moreno, V. *J. Inorg. Biochem.* **2007**, *101*, 660–666. (p) Fyles, T. M.; Tong, C. C. *New J. Chem.* **2007**, *31*, 655–661.

(6) For examples of triangles, see: (a) Fujita, M.; Aoyagi, M.; Ogura, K. *Inorg. Chim. Acta* **1996**, *246*, 53–57. (b) Schnebeck, R.-D.; Randaccio, L.; Zangrando, E.; Lippert, B. *Angew. Chem.* **1998**, *110*, 128–130; *Angew. Chem., Int. Ed.* **1998**, *37*, 119−121. (c) Lai, S.-W.; Chan, M. C.-W.; Peng, S.-M.; Che, C.-M. *Angew. Chem.* **1999**, *111*, 708–710; *Angew. Chem., Int. Ed.* **1999**, *38*, 669−671. (d) Habereder, T.; Warchhold, M.; Nöth, H.; Severin, K. *Angew. Chem.* **1999**, *111*, 3422–3425; *Angew. Chem., Int. Ed.* **1999**, *38*, 3225−3228. (e) Sun, S.-S.; Lees, A. J. *Inorg. Chem.* **1999**, *38*, 4181–4182. (f) Schneebeck, R.-D.; Friesinger, E.; Glahé, F.; Lippert, B. *J. Am. Chem. Soc.* **2000**, *122*, 1381–1390. (g) Yu, X.-Y.; Maekawa, M.; Kondo, M.; Kitagawa, S.; Jin, G.-X. *Chem. Lett.* **2001**, 168–169. (h) Schweiger, M.; Seidel, S. R.; Arif, A. M.; Stang, P. J. *Angew. Chem.* **2001**, *113*, 3575–3577; *Angew. Chem., Int. Ed.* **2001**, *40*, 3467−3469. (i) Lee, S. J.; Hu, A.; Lin, W. *J. Am. Chem. Soc.* **2002**, *124*, 12948–12949. (j) Fornies, J.; Gomez, J.; Lalinde, E.; Moreno, M. T. *Chem.−Eur. J.* **2004**, *10*, 888–898. (k) Gosh, S.; Turner, D. R.; Batten, S. R.; Mukherjee, P. S. *Dalton Trans.* **2007**, 1869–1871.

(7) (a) Drain, C. M.; Lehn, J. M. *J. Chem Soc., Chem. Commun.* **1994**, 2313–2315. (b) Romero, F. M.; Ziessel, R.; Dupont-Gervais, A.; van Dorsselaer, A. J. *J. Chem. Soc., Chem. Commun.* **1996**, 551–553. (c) Manna, J.; Whiteford, J. A.; Stang, P. J.; Muddiman, D. C.; Smith, R. D. *J. Am. Chem. Soc.* **1996**, *118*, 8731–8732. (d) Hall, J.; Loeb, S. J.; Shimizu, G. K. H.; Yap, G. P. A. *Angew. Chem.* **1998**, *110*, 130–133; *Angew. Chem., Int. Ed. Engl.* **1998**, *37*, 121−123. (e) Mukherjee, P. S.; Das, N.; Kryschenko, Y. K.; Arif, A. M.; Stang, P. J. *J. Am. Chem. Soc.* **2004**, *126*, 2464–2473. (f) Tarkany, G.; Jude, H.; Palinkas, G.; Stang, P. J. *Org. Lett.* **2005**, *7*, 4971–4973. (g) Das, N.; Gosh, A.; Arif, A. M.; Stang, P. J. *Inorg. Chem.* **2005**, *44*, 7130–7137. (h) Megyes, T.; Jude, H.; Grosz, T.; Bako, I.; Radnai, T.; Tarkanyi, G.; Palinkas, G.; Stang, P. J. *J. Am. Chem. Soc.* **2005**, *127*, 10731–10738. (i) Jude, H.; Disteldorf, H.; Fischer, S.; Wedge, T.; Hawkridge, A. M.; Arif, A. M.; Hawthorne, M. F.; Muddiman, D. C.; Stang, P. J. *J. Am. Chem. Soc.* **2005**, *127*, 12131–12139. (j) Jude, H.; Sinclair, D. J.; Das, N.; Sherburn, M. S.; Stang, P. J. *J. Org. Chem.* **2006**, *71*, 4155–4163. (k) Dias, H. V. R.; Gamage, C. S. P.; Keltner, J.; Diyabalanage, H. V. K.; Omari, I.; Eyobo, Y.; Dias, N. R.; Roehr, N.; McKinney, L.; Poth, T. *Inorg. Chem.* **2007**, *46*, 2979–2987.

peak broadening and hampers a detailed signal assignment. Finally, mass spectrometry often suffers from the fragmentation because of the weak coordinative bonds often supported by charge repulsion existing in multiply charged ions. Thus, it is not always clear, whether, for example, [3:3] complexes appearing in the mass spectra are a true solution component or a fragment from a bigger species.[9d] Coldspray ionization (CSI)[16]offers advantages here but is not always routinely available. In addition, unspecific aggregation during the Electrospray Ionization (ESI) process can lead to misinterpretation in that larger aggregates seem to form which are not present in solution.

In this Article, the equilibrium between squares and triangles is discussed to shed some more light on the problems associated with their analytical characterization. Elongated bis-pyridines **1** to **4** are used as the edge ligands together with (dppp)M(OTf)$_2$ (M = Pd^{II} **5**, Pt^{II} **6**) as the corners (Scheme 1). Only a combination of crystallography, different NMR methods, and mass spectrometry provides a complete picture of the associated equilibria and the dynamic processes occurring in solution. The utility of diffusion-ordered spectroscopy (DOSY NMR) is discussed in the context of dynamic processes interconverting different assemblies.

Results and Discussion

Synthesis. All assemblies presented in this article have been made by mixing stoichiometric amounts of the edge ligands **1**, **2**, **3**, or **4** and the corner complexes **5** or **6** in dimethylsulfoxide (DMSO) or dimethylformamide (DMF; Scheme 1). These two solvents had to be used for solubility reasons, when the edge ligands contained either urea or amide groups. Furthermore, a wide temperature range is accessible for variable-termperature NMR experiments in DMF. The mixtures were stirred for a couple of hours at room temperature before analysis to make sure that the equilibrium situation is monitored.

^{1}H and ^{31}P NMR Spectroscopy. The complexation of the pyridine nitrogens to the metal centers can be deduced from the complexation-induced signal shifts to higher field typically observed in the ^{31}P NMR spectra. A particularly reliable indicator of complex formation is the ^{195}Pt−P coupling constant of the pyridine complexes ($^1J_{Pt-P}$ = 3022−3045 Hz), which significantly differs from that of precursor **6** ($^1J_{Pt-P}$ = 3657 Hz). Clearly, two species exist in solution for **8a/b** and **12a/b** (Figure 1; insets) as indicated by the ^{31}P NMR spectra. A comparison of the ^{1}H NMR signals of the building blocks with those of the complexes reveals that small but significant chemical shift changes occur. A closer inspection of the ^{1}H NMR spectra also reveals two different sets of signals, some of which are superimposed. The ^{1}H NMR signals of the platinum complexes are sharper at room temperature than those of the palladium analogues (Figure 1). As we will see below, this can be rationalized by dynamic ligand-exchange processes whose rates depend on the metal centers and the ligands used.

DOSY NMR Spectroscopy and Molecular Modeling. To prove the simultaneous existence of squares and triangles in solution, Pulsed Field-Gradient Spin−Echo NMR (PGSE) experiments were performed. By measuring the diffusion coefficients, it is possible to determine the sizes of supramolecular compounds experimentally. The diffusion coefficients correlate with the size and the shape of the compounds. As a rough approximation, the different species under study were approximated as spheres, assuming that the fast rotation of the "discoidal" compounds on average leads to a sphere. With this approximation, the size of the different species can be calculated from the measured diffusion coefficients by the Stokes−Einstein equation (eq 1), where T is the absolute temperature, k_B the Boltzmann constant, r the hydrodynamic radius, and η the solvent viscosity at temperature T.[17]

$$D = k_B T/6\pi\eta r \quad (1)$$

As representative examples, we will discuss in detail only the results of the ^{1}H DOSY NMR spectra of **8a/b** and **12a/**

(8) For some examples see: (a) Beauchamp, D. A.; Loeb, S. J. *Chem. Commun.* **2002**, 2484–2485. (b) Tuna, F.; Hamblin, J.; Jackson, A.; Clarkson, G.; Alcock, N. W.; Hannon, M. J. *Dalton Trans.* **2003**, 2141–2148. (c) Graves, C. R.; Merlau, M. L.; Morris, G. A.; Sun, S.-S.; Nguyen, S. B. T.; Hupp, J. T. *Inorg. Chem.* **2004**, *43*, 2013–2017. (d) Jeong, K. S.; Kim, S. Y.; Shin, U.-S.; Nguyen, T. M. H.; Kogej, M.; Broekmann, P.; Jeong, N.; Kirchner, B.; Reiher, M.; Schalley, C. A. *J. Am. Chem. Soc.* **2005**, *127*, 17672–17685. (e) Kiplinger, J. L.; Pool, J. A.; Schelter, E. J.; Thompson, J. D.; Scott, B. L.; Morris, D. E. *Angew. Chem.* **2006**, *118*, 2090–2095; *Angew. Chem., Int. Ed.* **2006**, *45*, 2036−2041. (f) Clegg, J. K.; Lindoy, L. F.; McMurtrie, J. C.; Schilter, D. *Dalton Trans.* **2006**, 3114–3121. (g) Chand, D. K.; Biradha, K.; Kawano, M.; Sakamoto, S.; Yamaguchi, K.; Fujita, M. *Chem. Asian J.* **2006**, *1*, 82–90. (h) Cotton, F. A.; Murillo, C. A.; Stiriba, S.-E.; Wang, X.; Yu, R. *Inorg. Chem.* **2006**, *44*, 8223–8233. (i) Heo, J.; Jeon, Y.-M.; Mirkin, C. A. *J. Am. Chem. Soc.* **2007**, *129*, 7712–7713. (j) Baradjí, E. G.; Freisinger, E.; Costisella, B.; Schalley, C. A.; Brüning, W.; Sabat, M.; Lippert, B. *Chem.−Eur. J.* **2007**, *13*, 6019–6039. (k) Derossi, S.; Casanova, M.; Iengo, E.; Zangrando, E.; Stener, M.; Alessio, E. *Inorg. Chem.* **2007**, *46*, 11243–11253.

(9) (a) Lee, S. B.; Hwang, S.; Chung, D. S.; Yun, H.; Hong, J.-I. *Tetrahedron Lett.* **1998**, *39*, 873–876. (b) Schnebeck, R.-D.; Freisinger, E.; Lippert, B. *Eur. J. Inorg. Chem.* **2000**, 1193–1200. (c) Sautter, A.; Schmid, D. G.; Jung, G.; Würthner, F. *J. Am. Chem. Soc.* **2001**, *123*, 5424–5430. (d) Schalley, C. A.; Müller, T.; Linnartz, P.; Witt, M.; Schäfer, M.; Lützen, A. *Chem. Eur. J.* **2002**, *8*, 3538–3551. (e) Zhang, L.; Niu, Y.-H.; Jen, A. K.-Y.; Lin, W. *Chem. Commun.* **2005**, 1002–1004. (f) Cotton, F. A.; Murillo, C. A.; Yu, R. *Dalton Trans.* **2006**, 3900–3905. (g) Uehara, K.; Kasai, K.; Mizuno, N. *Inorg. Chem.* **2007**, *46*, 2563–2570.

(10) (a) Ferrer, M.; Mounir, M.; Rossell, O.; Ruiz, E.; Maestro, M. A. *Inorg. Chem.* **2003**, *42*, 5890–5899. (b) Ferrer, M.; Gutierrez, A.; Mounir, M.; Rossel, O.; Riuz, E.; Rang, A.; Engeser, M. *Inorg. Chem.* **2007**, *46*, 3395–3406.

(11) (a) Bark, T.; Düggeli, M.; Stoeckli-Evans, H.; Zelewsky, A. v. *Angew. Chem.* **2001**, *113*, 2924–2927; *Angew. Chem., Int. Ed.* **2001**, *40*, 2848−2851. (b) Mamula, O.; Monlien, F. J.; Porquet, A.; Hopfgartner, G.; Merbach, A. E.; Zelewsky, A. v. *Chem.−Eur. J.* **2001**, *7*, 533–539.

(12) Fujita, M.; Sasaki, O.; Mitsuhashi, T.; Fujita, T.; Yazaki, J.; Yamaguchi, K.; Ogura, K. *Chem. Commun.* **1996**, 1535–1536.

(13) Berben, L. A.; Faia, C. M.; Crawford, N. R. M.; Long, J. R. *Inorg. Chem.* **2006**, *45*, 6378–6386.

(14) Engeser, M.; Rang, A.; Ferrer, M.; Gutiérrez, A.; Schalley, C. A. *Int. J. Mass Spectrom.* **2006**, *255−256*, 185–194.

(15) (a) Lukoyanov, A. N.; Fedushkin, I. L.; Schumann, H.; Hummert, M. *Z. Anorg. Allg. Chem.* **2006**, *632*, 1471–1476. (b) Rang, A.; Engeser, M.; Maier, N. M.; Nieger, M.; Lindner, W.; Schalley, C. A. *Chem.−Eur. J.* **2008**, *14*, 3855–3859.

(16) (a) Sakamoto, S.; Fujita, M.; Kim, K.; Yamaguchi, K. *Tetrahedron* **2000**, *56*, 955–964. (b) Sakamoto, S.; Yoshizawa, M.; Kusukawa, T.; Fujita, M.; Yamaguchi, K. *Org. Lett.* **2001**, *3*, 1601–1604. (c) Tominaga, M.; Suzuki, K.; Kawano, M.; Kusukawa, T.; Ozeki, T.; Sakamoto, S.; Yamaguchi, K.; Fujita, M. *Angew. Chem.* **2004**, *116*, 5739–5743; *Angew. Chem., Int. Ed.* **2004**, *42*, 5621−5625. For a review, see: (d) Yamaguchi, K. *J. Mass Spectrom.* **2003**, *38*, 473–490.

Scheme 1. Self-Assembly of Interconverting Squares and Triangles from Simple Bis-pyridyl Building Blocks **1**−**4** with Different Spacer Lengths

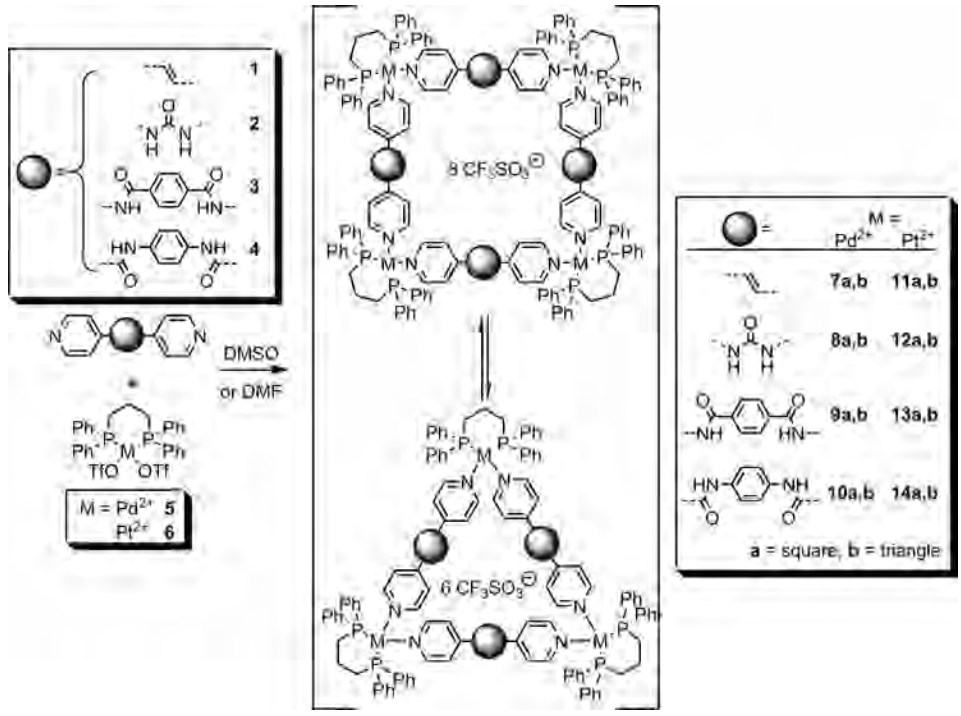

b. In all mixtures under study, the NH and *o*-pyridine protons are sufficiently separated from other signals so that they can easily be used for the DOSY measurements. Large structures have smaller diffusion coefficients than small ones. If squares and triangles coexist, two different sets of signals should thus be observed in the DOSY NMR spectra. Figure 2a shows the DOSY spectrum of **8a/b** at room temperature in DMSO-d_6. In the ^{1}H and ^{31}P NMR spectra, two sets of signals are clearly visible—a smaller one, which is tentatively assigned to the square, and a more intense one for the triangle. However, both sets of signals appear in the DOSY NMR spectrum with the same diffusion coefficient. This finding can be traced back to the three different time scales in the ^{1}H, ^{31}P, and DOSY NMR experiments. While the ligand exchange is slow on the ^{1}H and ^{31}P NMR experiments, it is fast on the DOSY time scale which works with a diffusion delay in its pulse sequence. At 273 K in DMF-d_7, the exchange becomes significantly slower so that two different diffusion coefficients for square and triangle can be determined for **8a/b** (Figure 2b). The diffusion coefficients calculated from the latter spectrum confirm the assignment of the square to the less intense signal and identifies the more intense signal with the triangle.

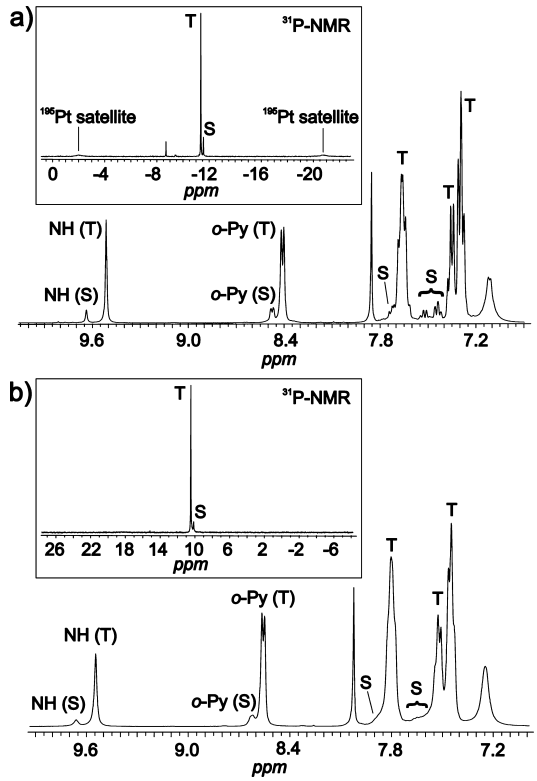

Figure 1. ^{1}H and ^{31}P NMR spectra of (a) **12a/b** and (b) **8a/b** (S = square, T = triangle).

For the analogous platinum complexes **12a/b**, two different diffusion coefficients were already observed in DMSO-d_6 at room temperature (Figure 2c). Clearly, the exchange between **12a** and **12b** is slow even on the DOSY NMR time scale under these conditions. This confirms the triangle-square exchange to be faster for the Pd than for the Pt compounds. Again, the less intense signal corresponds to the square. Qualitatively, the other complexes under study yield similar results. The experimental data of the ^{1}H DOSY NMR measurements of **7a/b** to **14a/b** are summarized in Supporting Information, Table S1.

For a comparison with the experimental radii obtained from the DOSY NMR experiments, the geometries of triangles and squares were optimized with the MM2 force-field implemented in the Cache program.[18] Different conformers have been explicitly considered in the calculations, although they have similar energies and geometry parameters

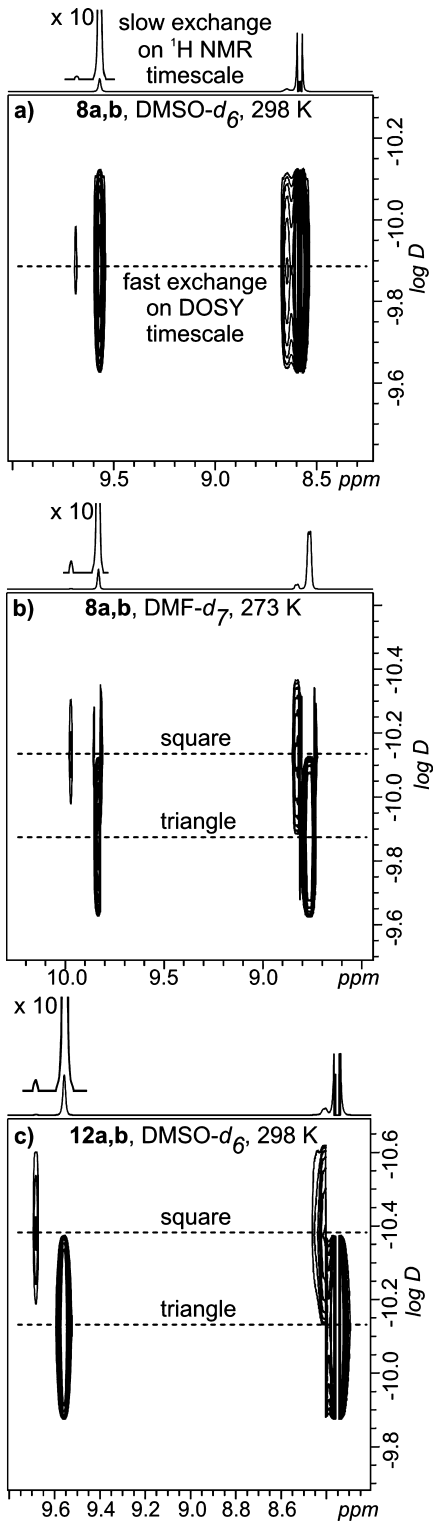

Figure 2. 2D DOSY NMR spectra of (a) **8a/b** recorded at 298 K in DMSO-d_6 (fast exchange), (b) **8a/b** recorded at 273 K in DMF-d_7 (slow exchange), and (c) **12a/b** recorded at 298 K in DMSO-d_6.

(defined in Figure 3 for **8a/b**). Consequently, we chose only the smallest conformer as a representative for determining the calculated geometry data summarized in Supporting Information, Table S1. Ligand **2** is slightly bent because of the central urea unit. Nevertheless, triangles and squares form rather than 2:2 complexes because the two pyridines at each metal corner prefer to adopt a geometry perpendicular to the

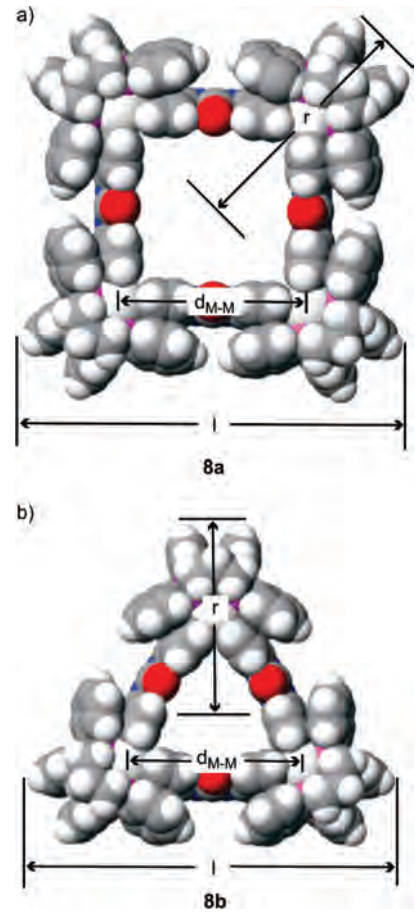

Figure 3. MM2 force-field-optimized structures of **8a/b** in space-filling representation. Only the largest of the different conformers is shown.

M−M−M−M plane. The ligand bending thus does not help to reduce strain in **8a/b** and **12a/b**.

In good agreement with the X-ray crystal structure data of triangle **7b** below, the calculated N−M−N angles of triangle **8b** are between 86.4° to 88.7° and thus are close to the expected value of 90°. This shows most of the triangle strain to be compensated by ligand bending (also see crystallography part below). The rigidity of the ligand plays thus an important role for the triangle-square equilibrium. In both structures in Figure 3, π-π interactions between each pyridine ring and one of the dppp phenyl rings are visible.

Three conclusions can be drawn from a comparison of the experimental and calculated radii. (i) The two species present in solution are triangles and squares. Even if the absolute, but approximate, experimental radii do not perfectly fit the calculation, the calculated radii of other possible species such as pentameric or hexameric complexes give a much worse agreement with the experimental data. (ii) Except for the lowest temperature (243 K), the experimentally determined radii are always somewhat smaller than the

(17) (a) Cohen, Y.; Avram, L.; Frish, L. *Angew. Chem.* **2005**, *117*, 524–560; *Angew. Chem., Int. Ed.* **2005**, *44*, 520−554. (b) Cohen, Y., Avram, L.; Evan-Salem, T.; Frish, L. Diffusion NMR in Supramolecular Chemistry. In *Analytical Methods in Supramolecular Chemistry*; Schalley, C. A., Ed.; Wiley-VCH: Weinheim 2007. (c) Macchioni, A.; Ciancaleoni, G.; Zuccaccia, C.; Zuccaccia, D. *Chem. Soc. Rev.* **2008**, *37*, 479–489.

(18) *CACHE 5.0 for Windows*; Fujitsu Ltd.: Krakow, Poland, 2001.

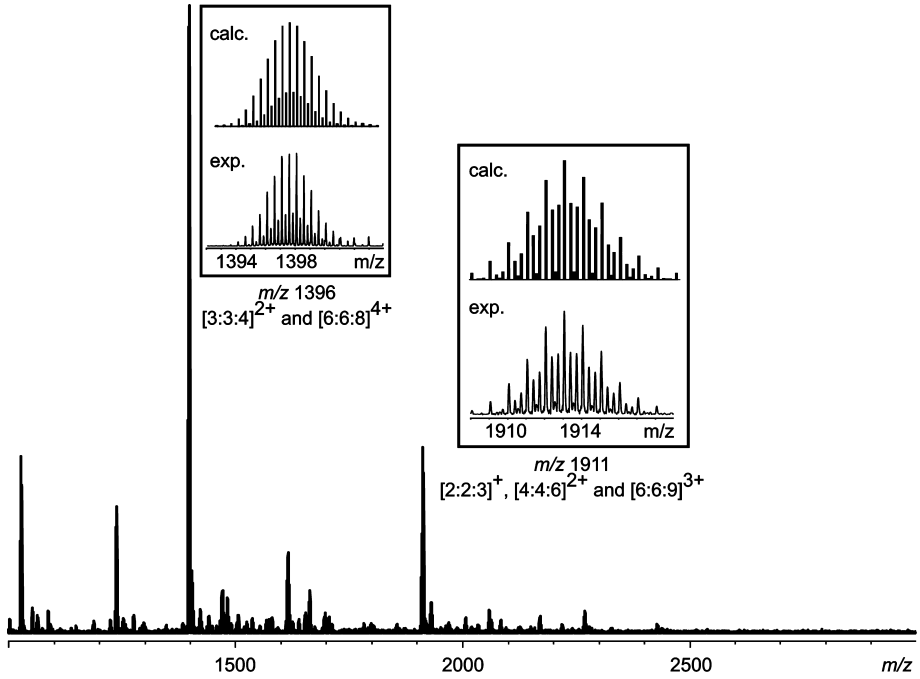

Figure 4. ESI-FTICR mass spectrum of **8a/b**. Signals are labeled by the $[m{:}l{:}c]^q$-nomenclature (see text). The insets compare the experimentally obtained isotope patterns with those simulated on the basis of natural isotope abundances.

calculated ones. This can be attributed to the approximation of the rather discoidal complexes as spherical ones and the cavity in the complex, which reduces the effective diffusion coefficient additionally. At 243 K, the experimental radii are larger than the calculated ones, likely because the viscosity of the solvent had to be extrapolated to this temperature. (iii) Irrespective of the solvent, the temperature, or the metal used, the squares always give smaller diffusion coefficients and therefore larger experimental radii than the corresponding squares.

Mass Spectrometry. Because of the weak coordinative bonds of our supramolecular assemblies, ESI is used as a soft ionization method. The compounds under study can be ionized in the ESI ion source by stripping off some counterions, thus generating complexes in different charge states. Figure 4 shows the electrospray ionization Fourier-transform ion-cyclotron resonance (ESI-FTICR) mass spectrum of **8a/b**. In addition to smaller peaks resulting from fragmentation of larger complexes, two major peaks are observed: (i) Signals for a singly charged $[2{:}2{:}3]^+$ fragment are superimposed with signals for doubly charged $[4{:}4{:}6]^{2+}$ (squares) and triply charged $[6{:}6{:}9]^{3+}$ (dimer of triangles) complex ions at *m*/*z* 1911 (in our $[m{:}l{:}c]^{q+}$-nomenclature, *m* stands for the number of *m*etal corners, *l* for the number of *l*igands, *c* for the number of *c*ounterions, and *q* for the number of charges). The $[4{:}4{:}6]^{2+}$ signals are quite weak indicating a small fraction of squares to be present. (ii) The other main peak at *m*/*z* 1396 corresponds to the superposition of quite abundant $[3{:}3{:}4]^{2+}$ complexes (triangle) and less abundant $[6{:}6{:}8]^{4+}$ complexes (dimer of triangles). Unspecific aggregation, which is the reason for the 6:6 complexes, is very typical for ESI-MS experiments of salts, and it is found for many similar species.[9d] One can think of these ions as anion-bridged dimers of cationic triangles mainly held together by electrostatic forces. In good qualitative agreement with the NMR spectra, the mass spectrum thus clearly exhibits more intense signals for triangles than for squares. A similar mass spectrum (Figure S1, Supporting Information) is observed for the analogous Pt compounds. The peak at *m*/*z* 1344 corresponds to a $[4{:}4{:}5]^{3+}$ square, which is not superimposed by other signals. Again, the signals for the triangles at *m*/*z* 1530 ($[3{:}3{:}4]^{2+}$) and *m*/*z* 3210 ($[3{:}3{:}5]+$) are more intense than those for the squares and superimposed by unspecific dimer ions. Fragmentation, however, is less pronounced for the Pt complexes as compared to the Pd complexes.

Temperature, Concentration, and Solvent Effects. Equilibria can be influenced significantly by changing temperature, concentration, or solvent. Similarly, the kinetics of the exchange processes may be altered by both parameters. Therefore, an examination of these effects is important to get a more complete picture of the complexes under study.

At 353 K, only one set of sharp, well resolved signals is observed in the NMR spectra of **8a/b** (Figure 5a), while two sets of signals appear at 273 K. The NH and *o*-pyridine protons are well separated, while most other signals are superimposed. Above the coalescence temperature is $T_c \approx$ 325 K (500 MHz), the equilibration of squares and triangles is fast on the NMR time scale for the Pd complexes. In the spectrum at 243 K, the signals are broader than those at higher temperatures. This can be traced back to the existence of different conformers which interconvert slowly at this temperature. Different conformers exist because of the chair-chair interconversion of the diphosphametallacyclohexane rings at each corner. At the same time, the dppp phenyl groups that stack with the pyridines hamper ligand rotation along the M−M axis. Both processes likely are slow on the NMR time scale now.

For the analogous platinum complexes **12a/b** (Supporting Information, Figure S2) no coalescence is observed even at

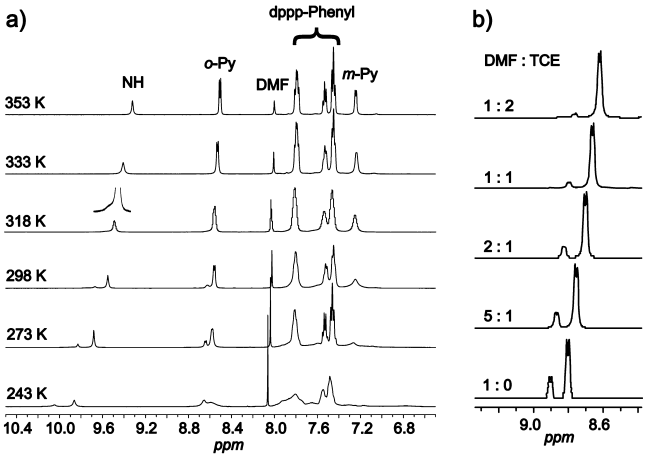

Figure 5. (a) Aromatic region of the variable-temperature ^{1}H NMR spectra (500 MHz) of **8a/b** recorded in DMF-d_7. (b) Partial ^{1}H NMR spectra (*o*-pyridine proton signals) of **7a/b** in various mixtures of DMF-d_7 and tetrachloroethane-d_2 at 298 K (all samples 20 mmol L^{-1}).

353 K. Consequently, the triangle-square equilibration is significantly faster for the Pd complexes in agreement with common knowledge that Pt(II) complexes are kinetically more stable than the Pd(II) analogues. In analogy to **8a/b**, broader signals are observed for **12a/b** at 243 K, which we again attribute to slow conformer equilibria. Similar behavior was detected for the other metal complexes generated by self-assembly with ligands **1**, **3**, and **4**. In all cases, the triangle-square equilibration is faster for the Pd complexes as indicated by the coalescence of NMR signals into one set at temperature clearly below 350 K. For the Pt complexes no coalescence up to 353 K is observed.

Because the *o*-pyridine protons appear separately for triangles and squares, quantitative data on the triangle-square equilibrium can be derived from their integration ratios and the initial concentration of the building blocks used. Because three squares can be converted into four triangles without changing the number of building blocks, eq 2 describes the equilibrium constant, from which the free enthalpies ΔG_{eq} for the equilibrium can be calculated. As this can easily be done at different temperatures, the enthalpic and entropic contributions can be obtained from a van't Hoff plot of ln K over $1/T$ (Supporting Information, Figure S3, eq 3).

$$K = \frac{[\text{triangle}]^4}{[\text{square}]^3} \quad (2)$$

$$\ln K = -\frac{\Delta G_{eq}}{RT} = -\frac{\Delta H_{eq}}{RT} + \frac{\Delta S_{eq}}{R} \quad (3)$$

This thermodynamic analysis was performed for **11a/b** (Table 1) because the available temperature range was too small for the other equilibria. At lower temperatures, the rather long equilibration times limit the experiment; for the Pd complexes, the temperature range is limited at the upper end through the coalescence discussed above. In the accessible temperature range, the triangles and squares were allowed to equilibrate until no integral changes were observed anymore. The data for **11a/b** is clearly consistent with the above discussion of enthalpic and entropic factors: The enthalpy for the conversion of three squares **11a** into four

Table 1. Thermodynamic Data for the **11a/b** Equilibrium (Experimental Errors ca. ±20%)[a]

T [K]	c(triangle) [mmol L^{-1}]	c(square) [mmol L^{-1}]	K [mol L^{-1}]	ΔG_{eq} [kJ mol^{-1}]
298	15.5	4.5	0.62	1.5
318	16.0	4.0	1.06	−0.7
333	16.8	3.2	2.56	−2.4
353	17.3	2.7	4.42	−4.7
373	17.9	2.1	10.33	−6.9

[a] ΔH_{eq} = 35.1 kJ mol^{-1}; ΔS_{eq} = 113 J mol^{-1} K^{-1}.

triangles **11b** is positive (ΔH_{eq} = 35.1 kJ mol^{-1}) reflecting the strain in the triangle structure. The entropic contribution is quite large and positive (ΔS_{eq} = 113 J mol^{-1} K^{-1}) and thus at elevated temperatures overcompensates the reaction enthalpy through a large $-T\Delta S_{eq}$ term. The positive entropy indicates that the reaction profits from the larger number of particles, when triangles are formed from squares.

The square/triangle ratio is also influenced by the building block concentration. For **8a/b** and **12a/b**, ^{1}H NMR spectra were recorded for solution concentrations between 2.5 mM and 20 mM. These two values limit the available concentration range because the signal-to-noise ratio decreases too much below 2.5 mM and the solubility of the urea squares prohibits examining solutions more concentrated than 20 mM. In this concentration range, a small but clearly visible shift of the square/triangle ratio is observed. For **8a/b**, it is <2:98 at 2.5 mM and 14:86 at 20 mM; for **12a/b**, we obtain 6:94 at 2.5 mM and 17:83 at 20 mM concentration (Supporting Information, Figure S4). The triangle is thus dominating the spectra over the whole concentration range.

Besides the temperature and concentration, the solvent is an important factor which influences the thermodynamics of the triangle-square equilibrium. For the NMR experiments reported so far, dipolar aprotic DMF-d_7 or DMSO-d_6 has been used as the NMR solvent. If more unpolar solvents such as tetrachloroethane-d_2 (TCE) are added, the equilibrium shifts toward the triangles. Figure 5b shows this for the **7a/b** equilibrium. Again, the *o*-pyridine protons provide the clearest picture. With stepwise increase of the TCE fraction, the signal assigned to the square decreases in favor of the triangle signal. A similar effect has been observed for the corresponding Pt complexes **11a/b**. The solvent mixture changes also the kinetic behavior in that the exchange processes proceed at lower rates with increasing TCE content of the sample. This is confirmed by coalescence temperatures increasing with TCE/DMF ratio. We attribute this finding to DMF molecules which support metal−ligand bond cleavages through their ability to donate an electron-pair into the empty coordination site formed in the intermediates.

Crystallography. Colorless, highly solvent-dependent single crystals suitable for X-ray analysis were grown by slowly diffusing benzene into an acetonitrile solution of a 1:1 mixture of the *cis*-coordinated platinum(II) corners **5** with *trans*-bis(4-pyridyl)ethene **1**. The X-ray crystal structure confirmed the formation of Pt triangles **11b** (Figure 6). It should be noted that NMR spectroscopy confirms both the triangles and squares to be present in acetonitrile as well (Supporting Information, Figure S5). The lattice of the crystal structure of **11b** includes five acetonitrile molecules for each

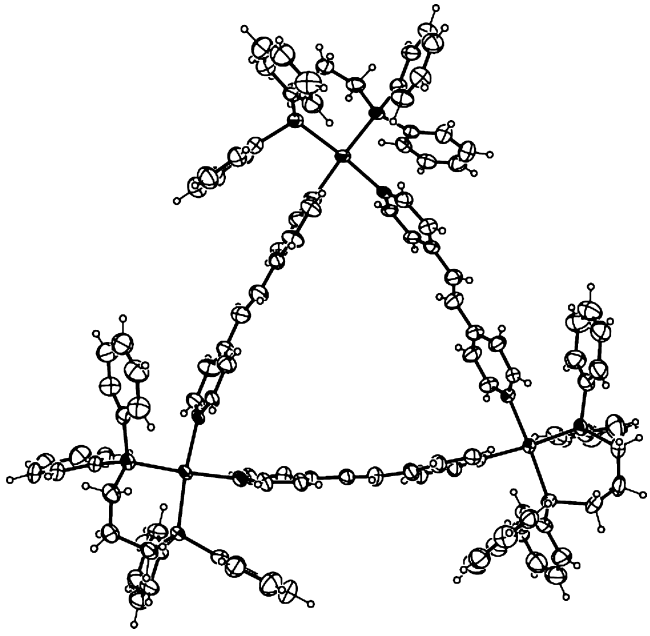

Figure 6. Oak Ridge Thermal Ellipsoid Plot (ORTEP; 50%-probability) of triangle **11b**. Anions and solvent molecules are omitted for clarity.

triangle in addition to the triangle itself and the six triflate counterions. In the structure analysis, some electron density remained unassigned because of high disorder. The packing of the triangles is shown in Figure 7. The cationic triangles form sheets that are further stacked on each other so that the disordered triflate anions are in between the cationic layers. Interestingly, the acetonitrile molecules are ordered to form a solvent cluster that runs through two stacked triangles belonging to upper and lower triangle sheets (Figure 7e).

The Pt−N bonds are all ∼0.21 nm long, and each N−Pt−N bond angle falls in the range of 83−85°. The bidentate phosphine bite angle is ∼92−93°. The angles around the Pt ion do not differ much from the ideal 90° and, as predicted by molecular modeling (see above), the ring strain of the triangle is mostly neutralized by bending the bis-pyridyl ethene ligands. Two planes defined by the two pyridine rings of each one of the ligands appear in the crystal structure with angles of 166° to 157° and thus deviate significantly from the expected, unstrained 180°. The Pt−Pt distances are 1.34 nm. The conformation and distances are similar to the previously reported triangle by Schweiger et al.[19] which bears trimethylphosphine platinum(II) corners. Schweiger et al. described that squares crystallized when the crystals were grown in the presence of small triflate counterions and that triangles were observed in the crystal when the mixture was crystallized in the presence of larger cobalticarborane anions. Unlike Schweiger et al., we never got crystals of the squares with our corners **5** and **6** that are definitively present in the solution equilibria. We attribute this to packing effects that are dominated by the nature of the corners. In addition to the crystal structure of **11b**, an analogous isomorphic structure of **7b** was obtained; the crystallographic data of **7b** is given in the Supporting Information cif file.

(19) Schweiger, M.; Seidel, S. R.; Arif, A. M.; Stang, P. J. *Inorg. Chem.* **2002**, *41*, 2556–2559.

Conclusions

Three important conclusions can be drawn from the results presented here. (i) A thorough analytical characterization of metallo-supramolecular complexes which can quickly interconvert requires the application of a number of different methods. From simple NMR experiments, we can only conclude that two different, highly symmetrical species are present but it remains unclear which ones. Mass spectrometry adds some information here but because of the formation of unspecific aggregates and fragments may lead to misinterpretations. Only the addition of DOSY NMR results on the diffusion coefficients and approximate radii of the complexes under study provides coherence here—at best, in combination with molecular modeling. On the basis of crystallography, one would arrive at the conclusion that triangles are formed exclusively, even for **7a/b** and **11a/b**, for which the amount of squares in solution is significant. Crystallization may prefer one component; the equilibrium readjusts the solution concentrations.

(ii) In this study, we presented bis-pyridyl ligands of different lengths and flexibility. Molecular modeling and crystallography agree that ligand bending is the major contribution to accommodate the strain. Consequently, the size of metallo-supramolecular squares cannot be increased easily by just extending the length of the ligands connecting the metal corners. When the ligand becomes long enough and therefore sufficiently flexible, triangles are entropically favored. The generation of larger squares thus would require a different strategy that takes into account the rigidity requirements that would prevent triangle formation. Simple squares formed according to Stang's self-assembly approach are thus limited to ligands not significantly longer than 4,4′-bipyridine itself.

(iii) The thermodynamic and kinetic behavior of the complexes discussed here is interesting in several respects. The equilibrium is affected by temperature in that entropy-favored triangles become more prominent at higher temperatures. It is also affected significantly by solvent polarity. Increasing amounts of nonpolar solvents result in an increased preference for triangle formation. For both, the Pd and Pt complexes, exchange reactions are observed which interconvert squares into triangles and vice versa. These processes depend on the nature of the metal. Pd complexes exchange more quickly than the Pt analogues. They also depend on solvent polarity. More polar solvents promote the exchange processes so that lower coalescence temperatures are observed in the temperature-dependent NMR spectra.

Experimental Section

Molecular Modeling. Molecular modeling was performed with the augmented MM2 force field implemented in the CaChe 5.0 program package.[18]

NMR Spectroscopy. ^{1}H, ^{13}C, and ^{31}P NMR spectra were recorded on Bruker DRX 500 (500, 126, and 202 MHz, respectively), DPX 400 (400, 100, and 162 MHz), and DPX 300 (300,

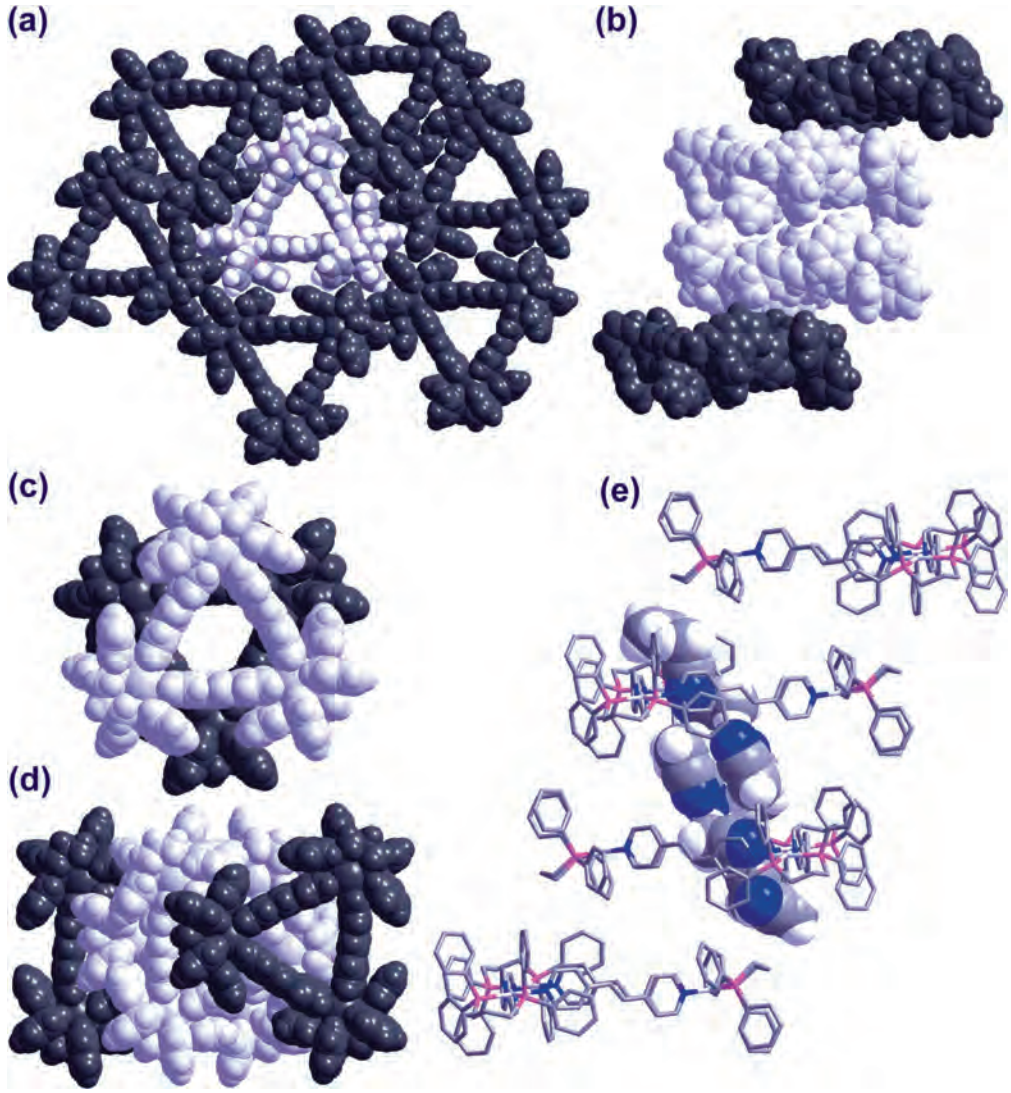

Figure 7. (a) Space-filling representation of a single triangle sheet in the crystal structure of **11b**. Each triangle is surrounded by six others by multiple π-π interactions. (b) The sheets pack on top of each other so that a cavity is formed by four triangles where the walls of the cavity are defined by two triangles (light gray), and it is further closed by the corners of upper and lower triangles (dark gray). (c) An image showing how the two cavity-forming triangles are stacked on top of each other (light and dark). (d) The cavity (light gray) is closed by the corners of the upper and lower triangles (dark gray). (e) The cavity is filled by a cluster of ten acetonitrile molecules. The disordered anions are omitted for clarity.

75, and 122 MHz) instruments with the solvent signals as internal standard. DOSY NMR spectra were recorded on a Bruker DMX 500 (500 MHz) with a *z*-gradient unit. For NMR experiments, 1:1 mixtures of palladium(II) or platinum(II) corner **5** or **6**, respectively, and ligand **1**−**4** were dissolved in 0.5 mL of deuterated DMF or DMSO to prepare a solution with a building block concentration of 20 mM.

ESI-FTICR Mass Spectrometry. ESI mass spectra were recorded on a Bruker APEX IV FT-ICR mass spectrometer with an Apollo electrospray ion source equipped with an off-axis 70° spray needle. The solutions for mass spectrometric analysis were prepared by mixing corner and ligand at 3 mM concentrations in DMSO followed by dilution with acetone to a concentration of about 300 μM to have a more suitable spray solvent. Analyte solutions were introduced into the ion source with a syringe pump (Cole-Parmers Instruments, Series 74900) at flow rates of about 3−4 μL/min. Ion transfer into the first of three differential pumping stages in the ion source occurred through a glass capillary with 0.5 mm inner diameter and nickel coatings at both ends. Ionization parameters were adjusted as follows: capillary voltage, +4.9 to +4.2 kV; end plate voltage, +4.5 to +3.7 kV; capexit voltage, −200 to −20 V; skimmer voltages, −5 to −25 V; and temperature of drying gas, 40 °C. The flows of the drying and nebulizer gases were kept in a medium range (ca. 25 psi). The ions were accumulated in the instrument's hexapole for 0.5−3 s, introduced into the FT-ICR cell, which was operated at pressures below 10^{-10} mbar, and detected by a standard excitation and detection sequence. For each measurement 16 to 64 scans were averaged to improve the signal-to-noise ratio.

Syntheses. The starting materials for the syntheses were used as purchased. Compounds **3**,[20] **4**,[21] **5**,[22,23] **6**,[4] **7a/b**,[9d] and **11a/b**[5] were prepared according to literature procedures.

N,N′-Bis(p-pyridyl)urea (2). A 480 mg quantity of (2.95 mmol) *N*,*N*′-carbonyldiimidazole were added to a solution of 500 mg (5.31 mmol) of 4-aminopyridine in 80 mL of dry toluene. The solution was heated to 80 °C for 3 h. Now, a second portion of 80 mg of (0.53 mmol) *N*, *N*′-carbonyl-diimidazole was added to the hot solution. After 30 more minutes of heating, the mixture was cooled down and stirred for 15 h at room temperature (rt). The resulting white precipitate was collected by filtration, washed with 50 mL of toluene and 50 mL of CH_2Cl_2, and dried in vacuo. A 350 mg

quantity of a white solid was obtained. Yield: 62%. ^{1}H NMR (400 MHz, DMSO-d_6): δ (ppm) = 9.27 (s, 2 H; NH); 8.39 (d, ^3J = 6.3 Hz, 4 H, $H_{o\text{-}py}$); 7.44 (d, $^3J_{H-H}$ = 6.3 Hz, 4 H, $H_{m\text{-}py}$). ^{13}C NMR (100 MHz, DMSO-d_6): δ (ppm) = 151.8, 150.1, 146.1, 112.5. High resolution EI-MS: m/z = 214.0864 (calc. m/z = 214.0855 for $[M]^{\bullet+}$).

Analytical Data of Squares and Triangles. Except for the signals of the NH- and *ortho*-pyridine-protons, which are separated for squares and triangles, all signals for both species are superimposed in the ^{1}H NMR spectra, so that it is not possible to assign them to individual complexes.

8a $C_{160}H_{144}F_{24}N_{16}O_{28}P_8Pd_4S_8$: 4124.9 g/mol, **8b** $C_{120}H_{108}F_{18}N_{12}O_{21}P_6Pd_3S_6$: 3093.7 g/mol. ^{1}H NMR (DMSO-d_6, 500 MHz, rt): square, 9.54; triangle, 9.43 (b, 8H, 11:89, NH); square, 8.38; triangle, 8.32 (d, ^3J = 5,8 Hz, 16H, $H_{o\text{-pyridine}}$); 7.63 (m, 32H, $H_{dppp\text{-}phenyl}$); 7.47 (m, 16H, $H_{dppp\text{-}phenyl}$); 7.38 (m, 32H, $H_{dppp\text{-}phenyl}$); 7.08 (b, 16H, $H_{m\text{-pyridine}}$); 3.12 (b, 16H, PCH_2); 2.01 (m, 8H, PCH_2CH_2) ppm. ^{13}C NMR (DMF-d_7, 126 MHz, rt): C_{arom}: 151.9 (S); 151.7 (T); 150.8 (S,T); 148.9 (S,T); 133.9 (S,T); 132.9 (T); 132.2 (S); 131.2 (S); 130.0 (T); 129.4 (S); 126.9 (S,T); 115.8 (S); 114.9 (T); 122.1 (CF_3); 22.4 (PCH_2); 18.2 ($PCH_2CH_2CH_2P$). ^{31}P NMR (DMSO-d_6, 202 MHz, rt): square, 9.50; triangle, 9.82 ppm. ESI-MS (positive mode, acetone): m/z = 2944.0 [**8b** − OTf]$^+$; 1913.1 [**8a** − 2OTf]$^{2+}$; 1397.6 [**8b** − 2OTf]$^{2+}$; 822.1 [**8b** − 3OTf]$^{3+}$.

9a $C_{188}H_{160}F_{24}N_{16}O_{32}P_8Pd_4S_8$: 4541.3 g/mol, **9b** $C_{141}H_{120}F_{18}N_{12}O_{24}P_6Pd_3S_6$: 3406.0 g/mol. ^{1}H NMR (DMSO-d_6, 500 MHz, rt): 10.77 (b, 8H, NH); 8.50 (b, 16H, $H_{o\text{-pyridine}}$); 7.95 (s, 16H, $H_{phenylen}$); 7.68 (m, 32H, $H_{dppp\text{-}phenyl}$); 7.50 (m, 32H, $H_{dppp\text{-}phenyl}$ + $H_{m\text{-pyridine}}$); 7.38 (m, 32H, $H_{dppp\text{-}phenyl}$); 3.15 (b, 16H, PCH_2); 2.04 (m, 8H, PCH_2CH_2) ppm. ^{13}C NMR (DMF-d_7, 126 MHz, rt): C_{arom}: 166.5 (S,T); 151.2 (S,T); 149.0 (S,T); 137.4 (S,T); 134.0 (S,T); 133.0 (S,T); 130.1 (S,T); 128.8 (S,T); 126.8 (S,T); 116.3 (S,T); 122.1 (CF_3); 22.5 (PCH_2); 18.5 ($PCH_2CH_2CH_2P$). ^{31}P NMR (DMSO-d_6, 202 MHz, rt): 10.90 ppm. ESI-MS (positive mode, acetone): m/z = 1553.7 [**9b** − 2OTf]$^{2+}$; 1364.5 [**9a** − 3OTf]$^{3+}$; 986.1 [**9b** − 3OTf]$^{3+}$.

10a $C_{188}H_{160}F_{24}N_{16}O_{32}P_8Pd_4S_8$: 4541.3 g/mol, **10b** $C_{144}H_{120}F_{18}N_{12}O_{24}P_6Pd_3S_6$: 3406.0 g/mol. ^{1}H NMR (DMSO-d_6, 500 MHz, rt): 10.44 (b, 8H, NH); 8.88 (b, 16H, $H_{o\text{-pyridine}}$); 7.71 (m, 64H, $H_{dppp\text{-}phenyl}$ + $H_{phenylen}$ + $H_{m\text{-pyridine}}$); 7.53 (m, 16H, $H_{dppp\text{-}phenyl}$); 7.43 (m, 32H, $H_{dppp\text{-}phenyl}$); 3.13 (b, 16H, PCH_2); 2.04 (m, 8H, PCH_2CH_2) ppm. ^{13}C NMR (DMF-d_7, 126 MHz, rt): C_{arom}: 151.4 (S,T); 144.2 (S,T); 135.8 (S,T); 134.0 (S,T); 133.2 (S,T); 130.2 (S,T); 126.2 (S,T); 123.9 (S,T); 121.4 (S,T); 122.1 (CF_3); 22.3 (PCH_2); 18.5 ($PCH_2CH_2CH_2P$). ^{31}P NMR (DMSO-d_6, 202 MHz, rt): square: 13.65; triangle: 10.00 ppm. ESI-MS (positive mode, acetone): m/z = 3256.5 [**10b** − OTf]$^+$; 2121.3 [**10a** − 2OTf]$^{2+}$; 1553.7 [**10b** − 2OTf]$^{2+}$.

12a $C_{160}H_{144}F_{24}N_{16}O_{28}P_8Pt_4S_8$: 4479.5 g/mol, **12b** $C_{120}H_{108}F_{18}N_{12}O_{21}P_6Pt_3S_6$: 3359.6 g/mol. ^{1}H NMR (DMSO-d_6, 500 MHz, rt): square, 9.98; triangle, 9.55 (s, 8H, 9:91, NH); square, 8.40; triangle, 8.34 (d, ^3J = 5.7 Hz,^3J = 6.3 Hz, 16H, $H_{o\text{-pyridine}}$); 7.66 (m, 32H, $H_{dppp\text{-}phenyl}$); 7.47 (m, 16H, $H_{dppp\text{-}phenyl}$); 7.40 (m, 32H, $H_{dppp\text{-}phenyl}$); 7.11 (b, 16H, $H_{m\text{-pyridine}}$); 3.22 (b, 16H, PCH_2); 1.99 (m, 8H, PCH_2CH_2) ppm. ^{13}C NMR (DMF-d_7, 126 MHz, rt): C_{arom}: 151.6 (T); 151.6 (S); 150.8 (S,T); 149.4 (S); 149.2 (T); 134.1 (S); 134.0 (T); 133.4 (S); 133.0 (T); 130.1 (S); 130.0 (T); 126.1 (S,T); 115.5 (S); 115.3 (T); 122.1 (CF_3); 22.4 (PCH_2); 18.3 ($PCH_2CH_2CH_2P$). ^{31}P NMR (DMSO-d_6, 202 MHz, rt): square, −12.04; triangle, −11.81 ($^1J_{Pt-P}$ = 3030 Hz) ppm. ESI-MS (positive mode, acetone): m/z = 3210.3 [**12b** − OTf]$^+$; 2090.3 [**12a** − 2OTf]$^{2+}$; 1530.2 [**12b** − 2OTf]$^{2+}$; 1343.9 [**12a** − 3OTf]$^{3+}$; 970.5 [**12b** − 3OTf]$^{3+}$.

13a $C_{188}H_{160}F_{24}N_{16}O_{32}P_8Pt_4S_8$: 4896.0 g/mol, **13b** $C_{141}H_{120}F_{18}N_{12}O_{24}P_6Pt_3S_6$: 3672.0 g/mol. ^{1}H NMR (DMSO-d_6, 500 MHz, rt): square, 10.87; triangle, 10.82 (b, 8H, 20:80, NH); square, 8.55; triangle, 8.51 (d, ^3J = 6.0 Hz, ^3J = 5.5 Hz, 16H, $H_{o\text{-pyridine}}$); square, 7.95; triangle, 7.93 (s, 16H, $H_{phenylen}$); 7.71 (m, 32H, $H_{dppp\text{-}phenyl}$); 7.51 (m, 32H, $H_{dppp\text{-}phenyl}$ + $H_{m\text{-pyridine}}$); 7.43 (m, 32H, $H_{dppp\text{-}phenyl}$); 3.25 (b, 16H, PCH_2); 2.02 (m, 8H, PCH_2CH_2) ppm. ^{13}C NMR (DMF-d_7, 126 MHz, rt): C_{arom}: 166.6 (S); 166.5 (T); 151.1 (S,T); 149.4 (S); 149.3 (T); 137.4 (S); 137.2 (T); 134.0 (S,T); 133.0 (S,T); 130.0 (S,T); 128.9 (S,T); 126.1 (S,T); 116.8 (S); 116.6 (T); 122.1 (CF_3); 22.4 (PCH_2); 18.3 ($PCH_2CH_2CH_2P$). ^{31}P NMR (DMSO-d_6, 202 MHz, rt): square, −11.88; triangle, −11.72 ($^1J_{Pt-P}$ = 3022 Hz) ppm. ESI-MS (positive mode, acetone): m/z = 2298.7 [**13a** − 2OTf]$^{2+}$; 1686.8 [**13b** − 2OTf]$^{2+}$; 1482.6 [**13a** − 3OTf]$^{3+}$; 1074.9 [**13b** − 3OTf]$^{3+}$.

14a $C_{188}H_{160}F_{24}N_{16}O_{32}P_8Pt_4S_8$: 4896.0 g/mol, **14b** $C_{141}H_{120}F_{18}N_{12}O_{24}P_6Pt_3S_6$: 3672.0 g/mol. ^{1}H NMR (DMSO-d_6, 500 MHz, rt): square, 10.40; triangle, 10.35 (b, 8H, 45:55, NH); square, 8.97; triangle, 8.93 (d, ^3J = 6.2 Hz, ^3J = 4.8 Hz, 16H, $H_{o\text{-pyridine}}$); 7.70 (m, 48H, $H_{dppp\text{-}phenyl}$ + $H_{phenylen}$); 7.54 (m, 32H, $H_{dppp\text{-}phenyl}$ + $H_{m\text{-pyridine}}$); 7.41 (m, 32H, $H_{dppp\text{-}phenyl}$); 3.30 (b, 16H, PCH_2); 2.06 (m, 8H, PCH_2CH_2) ppm. ^{13}C NMR (DMF-d_7, 126 MHz, rt): C_{arom}: 161.8 (S); 161.5 (T); 151.6 (S); 151.5 (T); 145.3 (S); 145.1 (T); 135.7 (S); 135.6 (T); 133.9 (S,T); 133.2 (S,T); 130.1 (S,T); 125.7 (S,T); 125.6 (S,T); 121.4 (S); 121.2 (T); 122.0 (CF_3); 22.1 (PCH_2); 18.2 ($PCH_2CH_2CH_2P$). ^{31}P NMR (DMSO-d_6, 202 MHz, rt): square, −12.40; triangle, −12.29 ($^1J_{Pt-P}$ = 3045 Hz) ppm. ESI-MS (positive mode, acetone): m/z = 3522.7 [**14b** − OTf]$^+$; 2298.8 [**14a** − 2OTf]$^{2+}$; 1686.8 [**14b** − 2OTf]$^{2+}$; 1482.6 [**14a** − 3OTf]$^{3+}$.

Crystallography. Data were recorded with a Nonius Kappa CCD diffractometer using graphite-monochromatized Mo Kα radiation [λ(Mo Kα) = 0.071073 nm)] and at 173.0 ± 0.1 K. The data were processed with Denzo-SMN v0.95.373,[24] and the structure was solved by direct methods.[25] Refinements based on F[25] were made by full-matrix least-squares techniques.[26] Empirical absorption correction based on multiple reflections was performed (Mulabs).[27] The hydrogen atoms were calculated to their idealized positions with isotropic temperature factors (1.2 or 1.5 times the C temperature factor) and refined as riding atoms. The atoms of the disordered triflate anions were treated isotropically as were the solvent atoms. In the final refinement of the solid-state structure of **11b**, there are 14 Q-peaks that could not be reasonably refined as atoms (between 1.1 and 3.5 e Å^{-3}) of which the four highest (2.5−3.4 e Å^{-3}) and three others (1.5−1.3 e Å^{-3}) are close to Pt atoms (1.1 Å) and the rest are close to badly disordered triflate anions. Electron density belonging to severely disordered solvent molecules was treated with the SQUEEZE-program.[28] This treat-

(20) Sun, S.-S.; Lees, A. J.; Zavalij, P. Y. *Inorg. Chem.* **2003**, *42*, 3445–3453.
(21) Pansanel, J.; Jouaiti, A.; Ferlay, S.; Hosseine, M. W.; Planeix, J.-M.; Kyritsakas, N. *New J. Chem.* **2006**, 71–76.
(22) Stang, P. J.; Cao, D. H.; Saito, S.; Arif, A. M. *J. Am. Chem. Soc.* **1995**, *117*, 6273–6283.
(23) Appleton, T. G.; Bennett, M. A.; Tomkins, I. B. *J. Chem. Soc., Dalton Trans.* **1976**, 439–446.
(24) Otwinowski, Z.; Minor, W. *Methods Enzymol.* **1997**, *276*, 307–326.
(25) Sheldrick, G. M. *Acta Crystallogr., Sect. A: Found. Crystallogr.* **1990**, *46*, 467–473.
(26) Sheldrick, G. M.; Schneider, T. R. *Methods Enzymol.* **1997**, *277*, 319–343.
(27) Blessing, R. H. *Acta Crystallogr., Sect. A: Found. Crystallogr.* **1995**, *51*, 33–38.
(28) Van der Sluis, P.; Spek, A. L. *Acta Crystallogr., Sect. A: Found. Crystallogr.* **1990**, *46*, 194–201.

ment resulted in a removal of electron density related to possibly one additional acetonitrile molecule. Solvent accessible void for **11b** is 221 Å^3

Crystal Data for 11b. Formula $Pt_3P_6C_{123}H_{108}N_6F_{18}S_6O_{18}\cdot 5NC_2H_3$, crystal size 0.1 × 0.15 × 0.2 mm, triclinic, space group $P\bar{1}$, a = 19.9254(6) Å, b = 21.0682(8) Å, c = 22.3641(8) Å, α = 67.792(2)°, β = 74.644(3)°, γ = 63.386(2)°, V = 7719.0(5) Å^3, Z = 2, ρ_{calcd} = 1.49 cm^{-3}, μ = 2.94 mm^{-1}, 90701 reflections measured, 28152 independent, 14932 used, number of parameters 1719, R_{int}= 0.113, $R1$ = 0.083 ($I > 2\sigma(I)$), $wR2$ = 0.190, GOF = 1.03. Minimum and maximum peaks in the difference map, −1.32 and 3.50 e Å^{-3}.

Crystal Data for 7b. Formula $Pd_3P_6C_{123}H_{108}N_6F_{18}S_6O_{18}\cdot 2.5NC_2H_3\cdot 2.75C_6H_5$ ($Pd_3P_6C_{183}H_{129}N_{8.5}F_{18}S_6O_{18}$), crystal size 0.15 × 0.20 × 0.50 mm, triclinic, space group $P\bar{1}$, a = 21.1746(4) Å, b = 21.2853(5) Å, c = 23.1441(5) Å, α = 96.687(1)°, β = 108.256(2)°, γ = 119.280(2)°, V = 8170.0 Å^3, Z = 2, ρ_{calcd} = 1.33 cm^{-3}, Mo Kα radiation, λ=0.71069 Å, μ = 0.54 mm^{-1}, T = 173 K, 105367 reflections measured, 28780 independent, 14350 used, number of parameters 1477, R_{int}= 0.137, $R1$ = 0.11 ($I > 2\sigma(I)$), $wR2$ = 0.28, GOF = 1.03. Minimum and maximum peaks in the difference map, −1.313 and 1.503 e Å^{-3}.

Acknowledgment. We thank the Deutsche Forschungsgemeinschaft (DFG), the Fonds der Chemischen Industrie (FCI), and The Academy of Finland (grant no. 122350) for funding. The Finnish Academy and the German Academic Exchange Service (DAAD) are acknowledged for supporting a Ph.D. student exchange program which made this project possible. We thank Dipl.-Chem. Alexander Rang and PD Dr. Burkhard Luy for help and interesting discussions on our work. C.A.S. thanks the FCI for a Dozentenstipendium.

Supporting Information Available: Some additional analytical data of the compounds. Crystallographic data in form of the cif file containing both structures. This material is available free of charge via the Internet at http://pubs.acs.org.

IC800334K